International Journal of Neural Systems, Vol. 24, No. 7 (2014) 1450025 (13 pages)

DOI: 10.1142/S0129065714500257

World Scientific
www.worldscientific.com

RETRIEVAL OF NOISY FINGERPRINT PATTERNS USING METRIC ATTRACTOR NETWORKS

MARIO GONZÁLEZ*
Universidad Estatal de Milagro, Milagro, Guayas, Ecuador
mgonzalezr1@unemi.edu.ec

DAVID DOMINGUEZ
Instituto de Fisica, Universidade Federal do Rio Grande do Sul
91501-970 Porto Alegre, RS, Brazil
david.dominguez@ufrgs.br

FRANCISCO B. RODRÍGUEZ
EPS, Universidad Autónoma de Madrid, 28049 Madrid, Spain
f.rodriguez@uam.es

ÁNGEL SÁNCHEZ
DCC-ETSII, Universidad Rey Juan Carlos, 28933 Madrid, Spain
angel.sanchez@urjc.es

Accepted 2 June 2014
Published Online 19 September 2014

This work experimentally analyzes the learning and retrieval capabilities of the diluted metric attractor neural network when applied to collections of fingerprint images. The computational cost of the network decreases with the dilution, so we can increase the region of interest to cover almost the complete fingerprint. The network retrieval was successfully tested for different noisy configurations of the fingerprints, and proved to be robust with a large basin of attraction. We showed that network topologies with a 2D-Grid arrangement adapt better to the fingerprints spatial structure, outperforming the typical 1D-Ring configuration. An optimal ratio of local connections to random shortcuts that better represent the intrinsic spatial structure of the fingerprints was found, and its influence on the retrieval quality was characterized in a phase diagram. Since the present model is a set of nonlinear equations, it is possible to go beyond the naïve static solution (consisting in matching two fingerprints using a fixed distance threshold value), and a crossing evolution of similarities was shown, leading to the retrieval of the right fingerprint from an apparently more distant candidate. This feature could be very useful for fingerprint verification to discriminate between fingerprints pairs.

Keywords: Attractor network; metric connectivity; small-world; fingerprint retrieval; sparse-coding; threshold dynamics.

1. Introduction

Fingerprints have been for more than one century the most important biometric method for the identification of persons.[1,2] This is due to the unique and permanent features present in the papillary ridges and valleys placed on the epidermic tip of the fingers. These features define a characteristic pattern for each person that is even differentiable for the case of monozygotic twins.[3] Using techniques from digital image processing, it is possible to automatically detect and measure the specific features present in the fingerprints like the minutiae, singular points or the direction and frequency of the ridges.

*Corresponding author.

Similar to other biometric authentication methods, two main modes of operation[4] are also applied for fingerprints: identification and verification, respectively. Identification is based on comparing the query or test fingerprint of one person to the corresponding ones of all enrolled classes or individuals of the database (it is a one-to-many problem) to determine the person identity corresponding to the query. Verification only performs just one comparison to determine the degree of similarity between a test fingerprint and a reference one to determine if both patterns correspond to the same individual (it is a one-to-one problem).

Like for other biometric modalities, the fingerprint image capture is the most critical stage in an automated fingerprint identification system since it determines the quality of the acquired fingerprint patterns and drastically influences the overall system performance.[1] Fingerprints images presenting a sufficient quality are characterized by distinguishable local and global structures[5,6] (i.e. defined texture-patterns of ridges and valleys within a local region and in the entire fingerprint). Similar structures can also be detected in palmprints.[7] Moreover, the quality of a biometric sample is related to its recognition/verification performance.[8] The different fingerprint sensing methods include both the usage of live optical or solid-state scanners (online capture) and the digitization of ink-rolled fingerprint images (offline capture).

Fingerprint patterns are commonly captured under controlled conditions during the enrollment stage and, in general, they have a good quality. These patterns can be efficiently compressed[9] for their storage in databases. However, during the testing stage (for recognition and/or verification tasks) the final user may not be taking care enough when interacting with the sensor in the intended real-world application of the biometric system. This could produce incomplete or noisy patterns that decrease the system performance due to operational aspects. Another type of wrong-comparison problem appears when it is necessary to match good-quality enrolled fingerprints to poor-quality latent ones (i.e. captured from a crime scene). In this scenario, a fully automatic matching process may not be possible due to bad ridge impressions, small finger area (i.e. lacking some minutiae points) and/or large nonlinear distortions present in the latent fingerprints.[8] In consequence, the current algorithms are semi-automatic and produce a reduced list of fingerprint candidates using the available information in the latent patterns, and then these candidates are checked by a human examiner to determine if any of the selected fingerprints is or not a match.[8]

Attractor Neural Network (ANN) models have been effectively applied in a wide range of situations, for example, shape recognition,[10] visual field data classification,[11] automotive traffic video analysis,[12] and brain-computer interface systems.[13] Metric ANNs are a Hopfield type of attractor networks using a metric connectivity distribution, i.e. small-world, which has a majority of local links with a moderate number of shortcuts. The shortcuts in the small-world networks with a short-term synaptic plasticity improve synchronization for the chemically coupled network.[14] Also, recent works[15–21] have shown that metric ANNs are able to sustain the existence of locally organized memories. The fingerprint patterns are examples of locally organized memories, with a well-defined spatial structure, the unique configuration of the ridges. The aim of this work is to analyze the learning and retrieval capabilities of the metric ANN when applied to collections of fingerprint images with different types and level of noise (see Fig. 1) in order to test the robustness of the proposed model. Metric connectivity is vital for real-world implementations,[12] where patterns are represented by spatially organized data that is, the information is nonuniformly distributed. Metric networks are expected to be more suitable to manage storing and retrieving of this type of structured patterns.[22] It is worthy of note that metric networks, being short-range architectures, are much cheaper in terms of the wiring cost than long-range ones. Our goal is to properly adapt the metric ANN model to the fingerprint retrieval problem by taking advantage of aspects like the involved metric and correlation matrices (i.e. the weights) together with a nonlinear dynamics (i.e. the adaptive thresholding strategy) with respect to a naïve static solution (consisting in matching two fingerprints using a fixed distance threshold value).

Some approaches of Hopfield neural networks for fingerprint identification, extract the information from the fingerprint minutiae, and use this information as input of the ANN.[23–25] Other approaches are holistic and use the fingerprint pattern keeping

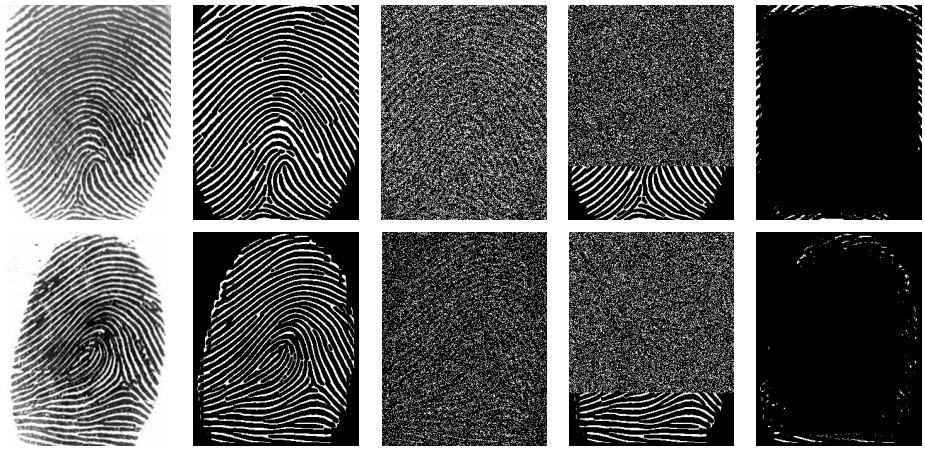

Fig. 1. From left to right: grayscale fingerprints, enhanced and binarized fingerprints ($a \sim 0.25$), uniform noise (initial condition $m^0 = 0.2$), localized noise ($m^0 = 0.2$), polygonal noise ($m^0 = 0.2$).

only a reduced region of interest (ROI),[26–29] due to the fact that computational resources demanded by the fully connected Hopfield neural network are high. Using diluted metric networks we can increase the ROI to cover almost the complete fingerprint. Besides, our method is holistic and minutiae extraction is not needed. The fingerprint pattern is directly used as input of the network. To our best knowledge, this work describes the first application of a metric ANN model to fingerprint retrieval. The influence of the overall model parameters (i.e. network topology, initial overlapping condition between query and learned patterns or threshold strategies) are also investigated in this paper. The proposed learning-retrieval method for collections of fingerprints presents as advantageous aspects the following ones:

(a) holistic approach: since there is no need from neither minutiae nor any other feature extraction stage (this can be convenient for matching of latent fingerprints where some parts of the patterns are lost);
(b) efficiency: the use of a metric network where the neurons have a reduced connectivity degree means smaller wiring and computational costs; and
(c) robustness: since the model can successfully handle with highly degraded (i.e. noisy or incomplete) fingerprint test patterns.

The novelty of the presented model, compared with metric ANN theoretical approaches dealing with structured information,[17] can be highlighted as follows: (1) 2D topology configurations. T-Grid, X-Grid and Cross-Grid configurations are employed for the small-world network, beyond the classic 1D-Ring approach (see Fig. 2). These 2D configurations better adapt for storing and retrieving fingerprint patterns. (2) Real-world patterns. For theoretical purpose, ANNs employ random patterns in order to avoid the interference (cross-talk term)

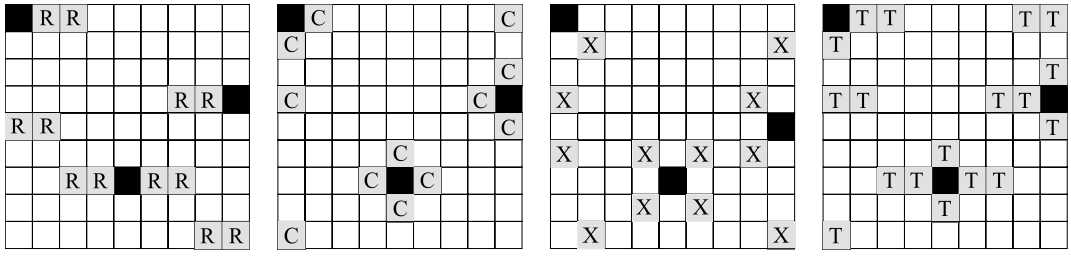

Fig. 2. Topology configurations tested (black=reference node, gray=neighbor nodes): Ring topology (left), C-Grid topology (middle left), X-Grid topology (middle right), T-Grid topology (right). $K = 4, \omega = 0.0$, except T-Grid with $K = 6$.

from patterns correlation. However, it is important to translate these models to real-world patterns, where one has to deal with added complexity, and we think it is novel to describe how to approach such real-world problems. This is achieved by fine tuning the model topological and dynamical parameters. (3) Overlap crossing. From the intrinsic dynamical properties of the model, it is possible to find the solution described as overlap crossing, retrieving the right fingerprint from an apparently more distant candidate.

The rest of the paper is organized as follows. Next, we describe the initial fingerprint pre-processing required. Section 3 introduces the components (i.e. topology and dynamics) of the proposed metric ANN model, and the measure of retrieval/similarity for the fingerprints patterns considered in our problem. Section 4 describes the experimental framework, and the characterization of the retrieval phases for the different noisy conditions tested, which are represented in a phase diagram. A "detective" problem (*overlap crossing*) is also described, where the network gives a satisfactory solution discriminating a supplanter fingerprint and evolving closely to the target from an intended fingerprint with a lower initial similarity, thanks to the dynamical nature of the network. Examples of latent fingerprint matching are presented, where the network manages to match the latent to the rolled fingerprint in a robust way, for different conditions such as stretched, incomplete and slightly rotated latent fingerprints. Finally, Sec. 5 outlines the conclusions of applying the present approach for fingerprint retrieval, and discusses the matter of its applicability and future work.

2. Fingerprint Pre-Processing

The fingerprint collections come from the International Fingerprint Verification Competition, editions FVC2000, FVC2002 and FVC2004 (see Ref. 30). Each edition has four different databases available, which are usually collected using the following sensors/technologies: optical, capacitive, thermal sweeping sensor, as well as synthetic generated fingerprints.

The fingerprint images are pre-processed as follows:

(1) Fingerprint image enhancement. The approach for fingerprint enhancement is based on the Short Time Fourier Transform (STFT) Analysis using MATLAB, as presented in Chikkerur *et al.*[31]
(2) Image binarization. The enhanced image is then binarized using the MATLAB image toolbox function **im2bw**, using as binarization threshold the output from the function **graythresh**.
(3) Morphological operations. The MATLAB function **bwmorph** applies morphological operations on binary images, and it has been employed with the following options:
    (a) Thin: It removes pixels so that an object without holes shrinks to a minimally connected stroke, and an object with holes shrinks to a connected ring halfway between each hole and the outer boundary.
    (b) Close: Performs morphological closing.
    (c) Clean and Spur: Removes isolated and spur pixels, respectively.
(4) Image cropping. Finally the images are cropped from an original resolution of 388×374, keeping the most of the fingerprint information, to a final resolution of 263×340 pixels. The boundary around the actual fingerprint impression is calculated and the borders with no information are cropped. Since the fingerprint borders may vary according to the capture conditions, the database mean fingerprint boundary size plus one standard deviation is kept, after the borders are cropped, to get the final resolution of all fingerprints.

The pre-processed patterns define the training set of enrolled fingerprints that the network will learn. These fingerprints are supposed to be captured during an off-line user-collaborative enrollment stage. Then different types of noise are applied to the training set (according to the description in Sec. 4.1, forming the test sets which simulate different capture conditions.

3. The Model

In this section, the metric ANN model is rigorously described, starting with the topology of the network and its learning (slow) and retrieval (fast) dynamics. Also, the information measures employed to determine the quality of the fingerprint retrievals are defined, as well as, the adaptive threshold strategy to

allow the network dynamics retrieve the fingerprint structured information.

3.1. *Topology and dynamics*

At any given discrete time step t, the network state is defined by a set of N-independent binary neuron variables $\boldsymbol{\tau}^t = \{\tau_i^t \in 0,1; i = 1,\ldots,N\}$, where 1 and 0 represent, respectively, active and inactive states. The network aims to recover a set of independent patterns $\{\boldsymbol{\eta}^\mu, \mu = 1,\ldots,P\}$ that have been stored by a learning process. That means, a stable retrieval state satisfies $\boldsymbol{\tau}^t = \boldsymbol{\eta}^\mu$, for large enough time t. Each pattern, $\boldsymbol{\eta}^\mu = \{\eta_i^\mu \in 0,1; i = 1,\ldots,N\}$, is a set of binary variables distributed according to the probability $p(\eta_i^\mu = 1) = a^\mu, p(\eta_i^\mu = 0) = 1 - a^\mu$, where $a^\mu = \langle \eta^\mu \rangle \equiv \sum_i \eta_i^\mu / N$ is the mean activity of each pattern.

The synaptic couplings between the neurons i and j are given by the adjacency matrix

$$J_{ij} \equiv C_{ij} W_{ij}, \tag{1}$$

where the topology matrix $\boldsymbol{C} = \{C_{ij}\}$ describes the connectivity structure of the neural network and $\boldsymbol{W} = \{W_{ij}\}$ is the matrix with the asymmetric learning weights. The topology matrix is split into local and random links. Local links connect a given neuron to its K_l neighbors, with periodic boundary conditions. Random links connect each neuron to K_r other neurons, uniformly distributed in the network. Hence the total number of connections, per neuron, is $K = K_l + K_r$. This way, the network topology is characterized by two parameters: the *connectivity* ratio and the *randomness* ratio, respectively defined by

$$\gamma = K/N, \quad \omega = K_r/K. \tag{2}$$

As in the *small-world* model,[32] the parameter ω plays the role of a rewiring probability. The storage cost of this network is $|\boldsymbol{J}| = N \times K$ if the matrix $\boldsymbol{J}$ is implemented as an adjacency list of K neighbors, and one would like to find out the behavior of the network in terms of these two parameters. An extremely diluted network is obtained as $\gamma \to 0$ and one restricts to this case in the paper. Three different 2D topology configurations, besides the classic 1D ring approach, are tested for the small-world network. The considered topologies Ring (Left), Cross-Grid (Middle-left), X-Grid (Middle-right), and T-Grid (Right) respectively, are represented schematically in Fig. 2.

For convenience, in the sequel one uses the normalized variables, the site and time dependence being implicit:

$$\sigma \equiv \frac{\tau - q}{\sqrt{Q}}, \quad \xi \equiv \frac{\eta - a}{\sqrt{A}}, \tag{3}$$

where $a \equiv \langle \eta \rangle, A \equiv \mathrm{Var}(\eta) = a(1-a)$, and $q \equiv \langle \tau \rangle, Q \equiv \mathrm{Var}(\tau) = q(1-q)$. Here, a and q are the pattern and neural activities, respectively. The averages done in this paper run over different ensembles, and are indicated in each case. These variables can be directly translated to those used in most works found in the literature for uniform (nonbiased) neurons,[15] in the case of $a = 1/2$.

In terms of these normalized variables, the retrieval of a pattern is achieved through the noiseless neuron dynamics

$$\sigma_i^{t+1} = g(h_i^t - \theta_i^t, q_i^t), \tag{4}$$

$$h_i^t \equiv \frac{1}{K} \sum_j J_{ij} \sigma_j^t, \quad i = 1,\ldots,N, \tag{5}$$

where h_i^t denotes the local field at neuron i and time t, and θ_i is its threshold of firing. The gain function is given by $g(x,y) \equiv [\Theta(x) - y]/\sqrt{y(1-y)}$, here the step function is used: $\Theta(x) = 1, x \geq 0, \Theta(x) = 0$, $x < 0$. In Eq. (4), it is introduced the average activity of the neighborhood of neuron $i, q_i^t = \langle \tau^t \rangle_i$, and its corresponding variance $Q_i^t = \mathrm{Var}(\tau^t)_i = \langle (\tau^t)^2 \rangle_i - \langle \tau^t \rangle_i^2$. The neighborhood average is defined as $\langle f^t \rangle_i \equiv \sum_j C_{ij} f_j^t / K$.

The weight matrix $\boldsymbol{W}$ is updated according to the Hebb's rule,

$$W_{ij}^\mu = W_{ij}^{\mu-1} + \xi_i^\mu \xi_j^\mu. \tag{6}$$

Weights start at $W_{ij}^0 = 0$ and after P learning steps, they reach the value $W_{ij} = \sum_\mu^P \xi_i^\mu \xi_j^\mu$. The learning stage displays slow dynamics, being stationary within the time scale of the faster retrieval stage, as described by Eq. (4). A stochastic macro-dynamics take place due to the extensive learning of $P = \alpha K$ patterns, where α is the load ratio.

3.2. *The information measures*

In order to characterize the retrieval ability, one needs to define appropriate information measures.[22]

In this case the overlap and neural activity,

$$m \equiv \frac{1}{N}\sum_{i}^{N}\xi_i\sigma_i, \quad q \equiv \frac{1}{N}\sum_{i}^{N}\tau_i, \tag{7}$$

which are the statistical correlation between the learned pattern ξ_i and the neural state σ_i, and the mean activity of the network, respectively, are enough to evaluate the network ability to retrieve a given pattern. When the pattern is successfully retrieved, $\tau_i = \eta_i$, $i = 1, \ldots, N$, one has $m \sim 1$ and $q \sim a$. Thus, the value of m can be taken as a degree of similarity between a test fingerprint and a reference one (stored by the network), in order to determine if both correspond to the same individual. If $m = 1$, one has a perfect matching between the two fingerprints; for $m = 0$, there is no match at all; for intermediate values, one may consider it a measure of how the two fingerprints match. If there is a match, the neural activity of the network must also agree with the fingerprint pattern activity. Together with the overlap and neural activity, one is interested in the load ratio $\alpha \equiv P/K$, that accounts for the storage capacity of the network. As the number of stored patterns grows the network is not able to retrieve them and the overlap goes to zero above a critical load ratio α_c.

3.3. *Threshold strategies*

In order to retrieve patterns with low activity (i.e. $a < 0.5$), it is necessary to use an adequate threshold for firing. If firing is not controlled, the neural activity could be higher (lower) than the pattern activity, whenever the threshold is too small (large). The more sparse is the code, more sensible is the interval where the threshold can move on. One can search for a threshold which is a function of the load ratio, the pattern activity, the randomness and the connectivity parameters. In particular, one could think about a dynamical threshold, which is updated for each retrieval time step.[33] Also, neural variability in the form of threshold variability (i.e. heterogeneous thresholds) contribute to low error discrimination in some tasks.[34] A self-control threshold that works for very low activities was proposed in the sparse-coding literature.[35]

Here, the following strategy θ^t is proposed:

$$\theta_i^t = \begin{cases} \theta_0^t, & q_i^t < 0.5, \\ -\theta_0^t, & q_i^t > 0.5. \end{cases} \tag{8}$$

The value of the θ_0 can be estimated as a function of the mean activity of the patterns set, $\theta_0(\bar{a}) = \frac{1-2\bar{a}}{2\sqrt{\bar{A}}}$. Here, $\bar{a} = \langle a^\mu \rangle_\mu$, is the mean activity over all patterns and $\bar{A} = \bar{a}(1-\bar{a})$ is its variance. A detailed explanation on calculating the dependence on the pattern sparseness can be found in Dominguez *et al.*[17]

Additionally, one can define an additional parameter ρ, with an empirical value of $\rho = 0.7$, and define $\theta_0^t = \rho\theta_0$ for the first time steps (say $t < 20$), so that, the network avoids getting trapped in spurious minima at the beginning of the network updating. For $t > 20$, one has $\theta_0^t = \frac{1}{\rho}\theta_0$ so that the higher threshold stabilizes the attained state. For $\theta_0(\bar{a} = 0.2258) \approx 0.66$, one has $\theta_0^t \approx 0.46$, $t < 20$, and $\theta_0^t \approx 0.94$, $t > 20$.

4. Results: Attractor Properties

In this section, the main results of the work are presented, starting with the characterization of the retrieval performance of the network in terms of the load parameter α for all topology configurations explored. Then, the phase diagrams showing the retrieval behavior for the parameters $\omega \times \alpha$ is depicted for all topology configurations and initial conditions. Finally, all conditions in which the *overlap crossing* occurs are delimited and examples are presented.

4.1. *Retrieval performance*

In order to consider a realistic system application scenario, in our approach, the learned patterns are intended to be captured during an off-line user-collaborative enrollment stage and consequently these fingerprint images present a high quality. On the other hand, the query (or test) patterns are recreated using the fingerprint images of the training set (see Sec. 2) but adding them some different types and levels of degradations. These are respectively referred as: "uniform noise" where the fingerprint is randomly added an amount of salt-and-pepper noise, "polygonal noise" where some nonregular regions of a given fingerprint are removed from a fingerprint image, and "localized noise" where a test pattern is created by combining a small regular portion of a rolled fingerprint and the rest of the pattern is completed with independent salt-and-pepper noise. These degraded types of tests patterns simulate some

realistic capture conditions of the query fingerprints images that can be due to sensor noise captured in image acquisition (for the case of the uniform noise) or to a nonappropriate interaction of the final user with the sensor (for the case of the polygonal or the localized noise). In general, the fidelity of the rolled (learned) patterns to the fingers is very high while the corresponding one for the test templates to the source finger is low. Consequently, the general low-degree of statistical correlation between the learned patterns and their corresponding query ones will make it difficult the considered retrieval problem for the different kinds of noisy patterns.

Figure 1 shows two examples of fingerprints with the different types of noise used as initial conditions by the network. From left to right are presented the grayscale image obtained from the sensor, the enhanced and binarized fingerprint, the uniform salt-and-pepper noisy fingerprint, the localized noisy fingerprint, and finally the polygonal noisy fingerprint where the missing regions are generated with the MATLAB poly2mask function, which computes a binary region polygonal mask. The fingerprint collection intended to store and retrieve, is characterized with a mean activity of $\bar{a} = 0.2258$, that is, one has $\theta_0\,(\bar{a} = 0.2258) \sim 0.66$ for the threshold retrieval dynamics. This threshold will be used throughout the whole work, unless stated otherwise.

The small-world network retrieval abilities are tested for the different topology configurations that are represented schematically in Fig. 2. These considered topologies are: Ring (Left), Cross-Grid (Middle-left), X-Grid (Middle-right), and T-Grid (Right), respectively. Here, the network parameters are $K = 4$ and $\omega = 0.0$ except T-Grid with $K = 6$ in the right panel. Here the T-Grid configuration is built considering the horizontal neighbors as twice the vertical ones $K_h = 2 \times K_v$. The network dilution is an important factor that determines the number of patterns the network is able to store and retrieve ($P \equiv \alpha K$). It is also critical from a computational point of view, given that the learning/retrieving time is of order $O(N \times K \times P)$. Empirically, $K = 200$ represents a good trade-off between the computational cost and the storage capability of the studied networks. We use in all the following $\gamma = K/N = 200/89{,}420 \sim 0.0022$.

In Fig. 3, the stationary states m^* reached by the network, are plotted as a function of the load ratio α, for different values of the topological parameter ω. The simulations results are plotted for a network with $N = 340 \times 263 = 89{,}420$ (which corresponds to the spatial resolution of the fingerprint image), and $K = 200$. In order to study the properties of the attractor basins for the stationary states, we study the retrieval capacity for uniform noisy fingerprints as initial condition. The network initial state correspond to a uniform salt-and-pepper noisy condition with $m^0 = 0.2$. The network evolves for $t = 100$ to a stationary state with overlap m^*, which is depicted in function of the load ratio α, for different values of the topological parameter ω. The stationary overlaps m^* are represented with symbols and the solid lines represent the corresponding smooth averaged curves.

In the right panel, for the T-Grid topology with $\omega = 1.0$, the network has a critical load ratio of $\alpha_c \sim 0.13$. For intermediates values, i.e. $\omega = 0.6$ the network has a better performance than the random

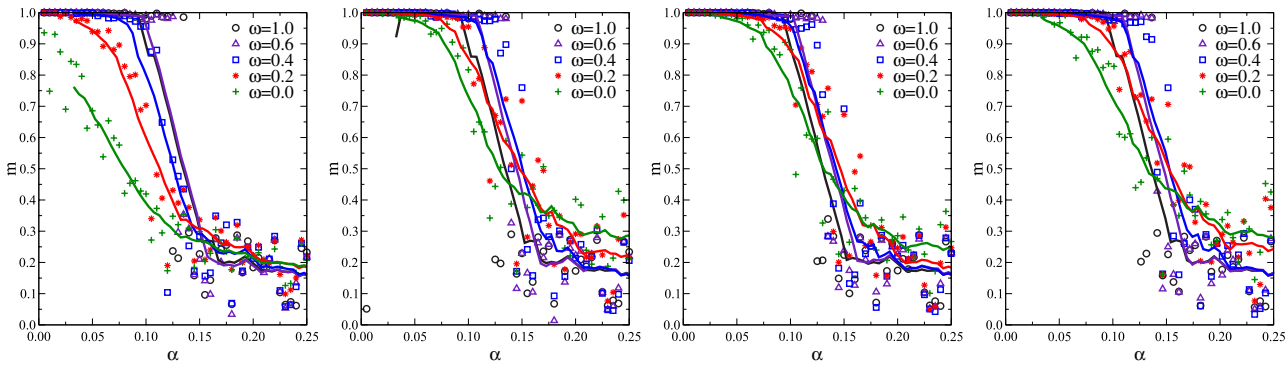

Fig. 3. Retrieval capacity of uniform noisy fingerprints for different values of the randomness parameter ω, with $N = 89{,}420$, $K = 200$ and initial condition $m^0 = 0.2$. Left: Ring topology. Middle-left: C-Grid topology. Middle-right: X-Grid topology. Right: T-Grid topology.

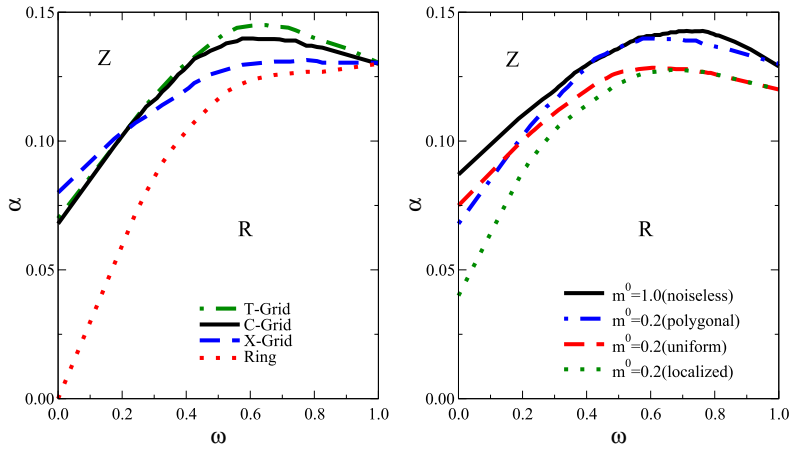

Fig. 4. Phase diagrams ($\omega \times \alpha$), networks with $N = 89{,}420$, $K = 200$. $R \equiv$ Retrieval phase below the curves. $Z \equiv$ no information above the curves. Left: Phase diagram for the different topology configurations studied: T-Grid (dot-dashed line), C-Grid (solid line), X-Grid (dashed line), Ring (dotted line), with initial condition $m^0 = 0.2$ polygonal noise. Right: C-Grid topology tested for different initial conditions: noiseless $m^0 = 1$, $m^0 = 0.2$ polygonal noise (dot-dashed line), $m^0 = 0.2$ uniform noise (dashed line), and $m^0 = 0.2$ localized noise (dotted line).

network ($\omega = 1.0$) achieving $\alpha_c \sim 0.145$. The local network with $\omega = 0.0$ has the lowest performance with $\alpha_c \sim 0.068$. For the C-Grid and X-Grid, in the middle panels a similar behavior can be appreciated. However, for the Ring topology in the left panel, the network for the intermediate value of $\omega = 0.6$ only manages to perform as well as the random network $\omega = 1.0$. For $\omega < 0.6$, the Ring topology configuration has a poor performance as clearly shown in the left panel. We have tried other 2D topologies, like a full-square of neighbors, and a larger T-structure, and the results are similar to that shown in Fig. 3 for the C-Grid and X-Grid configurations. All 2D-topology configurations proved to adapt better to the type of spatially structured patterns studied here, the fingerprints, with the T-Grid performing better than the C-Grid and X-Grid configurations. The metric of the network plays an important role, to choose an intermediate value of ω is also decisive given that the patterns have a spatially distributed information.

4.2. *Phase diagrams and network dilution*

According to the definition of the order parameter m, and following the results presented in the previous subsection, the stationary states of the network can be defined. The network may exhibit either *retrieval* (R) phase, with $m^* \neq 0$, and a *zero* (Z) phase with $m^* = 0$, without any information. Strictly, we consider the retrieval phase R for $m^* > 0.9$, and the Z phase (no retrieval) for $m^* < 0.9$ in order to identify both regions of the phase diagrams in Fig. 4. When the network starts in the vicinity of a pattern, it will move closer to that pattern if the load ratio is lower than that of the retrieval saturation, represented by the $\alpha_R(\omega)$ curves. In order to study the retrieval phase, extensive Monte Carlo simulations of the system were performed with $K = 200$ and $N = 89{,}420$ neurons.

In Fig. 4-left, is depicted a phase diagram for the different topology configurations (T-Grid, C-Grid, X-Grid and Ring) described schematically in Fig. 2. The initial condition is $m^0 = 0.2$ polygonal noise. One can appreciate that the Ring configuration performs poorly for low values of ω when compared with the 2D-Grid configurations. One can appreciate a region where the T-Grid configuration performs better than the X-Grid and C-Grid for values of $\omega > 0.4$. For $\omega < 0.2$, is the X-Grid configuration which performs better for low values of ω, adapting better to the fingerprint spatial configuration when the majority of the connections is local. One can observe an optimal value for the T-Grid configuration around $\omega \sim 0.65$. Although, the network perform as well as the random configuration ($\omega = 1.0$) for values as low as $\omega = 0.4$.

In Fig. 4-right, the separation between the R retrieval phase and Z no information phases are

depicted for the different initial conditions studied in this work. There is a transition from the Z to R phases at the $\alpha_R(\omega)$ curves, represented by the solid and the different discontinued lines, below which the phase of retrieval information is stable. The network retrieval of noisy fingerprints is robust, that is, the basin of attraction of the network is very large for this type of fingerprint patterns, as shown by the transition curves (discontinued lines) from the Z to R phases for the different noisy initial conditions: polygonal, uniform, and localized noise, respectively, all with an initial condition with $m^0 = 0.2$. For the noiseless initial condition ($m^0 = 1.0$), as well as, for the different noisy initial conditions, the phase diagram shows that a network with local connection plus random shortcuts, i.e. $0.6 < \omega < 0.7$, performs better than the random one ($\omega = 1.0$).

In Fig. 5 is presented the retrieval performance of the metric ANN, with $N = 89{,}420$ and Ring topology configuration, for extreme values of $\omega = 0.0$ and $\omega = 1.0$, and increasing values of network degree K. One can observe that the critical load decreases from $\alpha = 0.055$ to $\alpha = 0.003$ for $\omega = 0.0$, and from $\alpha = 0.130$ to $\alpha = 0.008$ for $\omega = 1.0$, going from an average of 20 min to around 500 min of execution time. That is equivalent to double the storage capacity from 26 patterns to 54 in the case of the random network ($\omega = 1.0$), by expending 25 times the computation time. The fully connected network is not computationally feasible for the fingerprint size selected in this work. In order to keep the most of the fingerprint impression, very diluted connectivity is needed. Other ANN approaches using full connectivity, use only a reduced ROI of the fingerprint pattern to avoid the computational cost.[26–29] For the simulations we have used a computer cluster system with 4 Opteron Abu Dhabi 6344 CPU, 12 cores at 2.6 GHz and 128 GB of physical memory per node.

Also, a quantitative comparison of the accuracy of our model with classic methods using features at Level 1 (macrodetails, e.g. pattern type), Level 2 (namely, minutiae), and Level 3 (microdetails, e.g. sweat pores),[8] is not straightforward. The presented approach is holistic, considering all the fingerprint features Levels as a whole. However, one may consider the accuracy of the system considering (1) the retrieval overlap value m as the degree of similarity between a pair of fingerprints, as mentioned above, and (2) $P_c = \alpha_c \times P$ as the number of correctly recognized fingerprints. It is worth to notice that increasing the network degree K, the network is able to store a larger number of patterns but at high computational costs.

4.3. *Overlap crossing*

Since the present model is a set of nonlinear equations, it is worth to study the properties of the attractor basins for the stationary states. In order to apply it to a "detective" problem, we study the evolution of the network starting from an initial condition $\sigma^{t=0}$, which has small but finite overlap $m^t \equiv < \sigma^t \xi >$ with two learned patterns (fingerprints), say ξ_1 and ξ_2, so that $m_1^{t=0} < m_2^{t=0}$. Although an easy straightforward comparison between the initial state and both fingerprints leads to a naïve conclusion that the right fingerprint is ξ_2, after the network evolves, the adaptive threshold dynamics shows that the closer

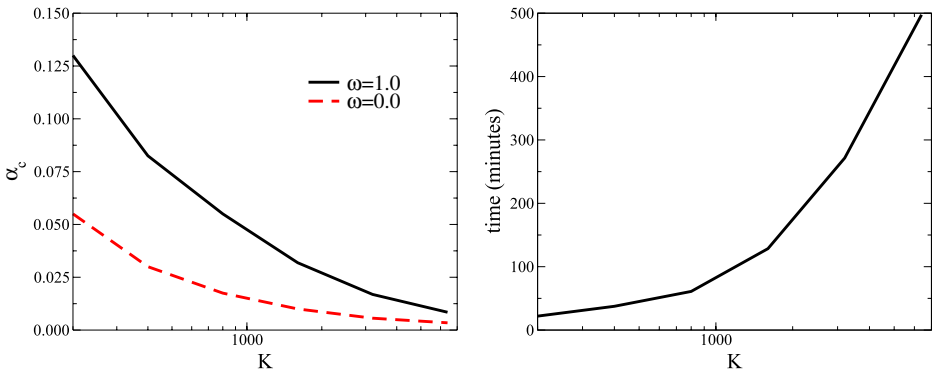

Fig. 5. Left: Critical load α_c of the ANN for increasing values of K and extreme values of $\omega = 0.0$ and $\omega = 1.0$. Right: Computation time for increasing values of network degree K. Network with $N = 89{,}420$ and Ring topology configuration.

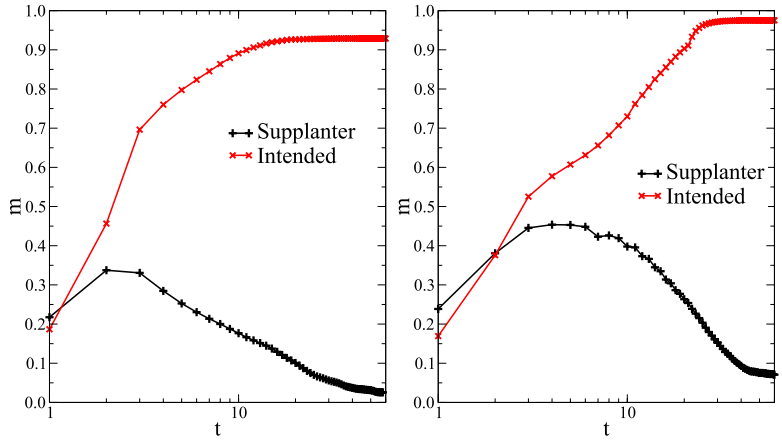

Fig. 6. Overlap crossing. Network with: $N = 89{,}420, K = 200, \omega = 0.3, \theta_0 = 0.4, \alpha = 0.05$ (*left*) and $\alpha = 0.1$ (*right*). Cross-symbol line: Supplanter overlap evolution. X-symbol line: Intended overlap evolution.

pattern (the better fingerprint match) is in fact ξ_1, because $m_1^* > m_2^*$.

Figure 6-left depicts the overlap crossing between two given patterns, say $\{\xi_1, \xi_2\}$, for a network with: $N = 89{,}420, K = 200, \omega = 0.3$, and X-Grid topology configuration, with a load ratio $\alpha = 0.05$ and neural threshold $\theta_0 = 0.4$. When the network starts in a state corresponding to the supplanting fingerprint, with an initial overlap of $m^0_{\text{sup}} \sim 21.8\%$, in a logarithmic time scale (t) the network evolves to a final state with a final overlap of $m^*_{\text{sup}} = \sim 2.58\%$ with the reference fingerprint. When the network starts in a state corresponding to the intended fingerprint with a lower initial overlap of $m^0_{\text{int}} = \sim 18.7\%$, one can appreciate the occurrence of an overlap crossing, when in a logarithmic time scale (t), the network evolves to a final network state with a higher overlap value of $m^*_{\text{int}} \sim 93.9\%$ with the reference fingerprint. A similar behavior is observed for a larger load ratio $\alpha = 0.1$ as shown in Fig. 6-right. The network gives a satisfactory solution to the "detective" problem, discriminating the supplanter fingerprint and evolving closely to the reference one from an intended fingerprint with a lower initial overlap.

In order to take place an overlap crossing the network must have a metric structure with $\omega < 0.4$. Also, a neural threshold between $0.25 \leq \theta_0 \leq 0.6$ is necessary for the overlap crossing. This neural threshold, slightly lower than the optimal $\theta_0 = 0.66$, lets the network dynamics scape from the supplanter state. Finally, an initial overlap $m^0_{\text{int}} \geq 0.15$ is needed for the crossing to occur, and the difference between m^0_{sup} and m^0_{int} can be up to 10%. Observe that the present model has a time-discrete synchronous dynamics which allows the crossing of trajectories for deterministic update of the m^t macroscopic parameter. Thus, the solid lines in Fig. 6 are guides for the eyes in order to observe visually this crossing in a clearer way.

The detective example of overlap crossing, can be seen as a case of separating latent overlapped fingerprints, where one can extract the intended fingerprint from an overlapped impression, that have a close initial similarity m with two fingerprints. Separating overlapped fingerprints is very challenging in practice. Feng *et al.*[37] propose robust algorithms for estimating component orientation fields, in order to separate the overlapped latent fingerprints. For poor quality impressions, Zhao and Jain[38] propose modeling fingerprint orientation fields from manually marked clues, for reconstruction purposes, enhancing the separation and matching accuracy of overlapping fingerprints. The dynamical properties of the proposed metric network would allow such discrimination, separating overlapped fingerprints as shown by the detective example in Fig. 6.

4.4. *Matching latent fingerprints*

Figure 7 shows examples of latent fingerprints retrieval for a network $N = 89{,}420$, $K = 200$, $\omega = 0.4$, and T-Grid topology configuration. A set of rolled fingerprints (top panels of Fig. 7) is stored by the network during the learning process for a pattern load $\alpha = 0.05$. A set of latent fingerprints is used as initial condition of the network (see Table 1). Latent

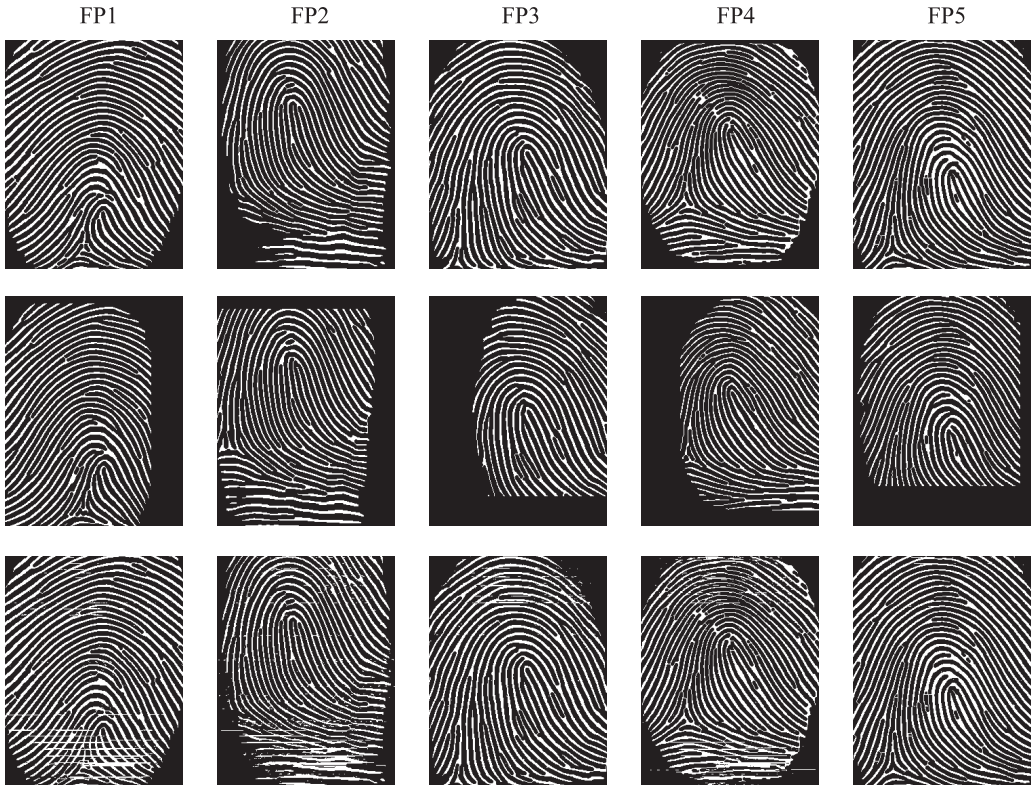

Fig. 7. Latent fingerprint retrieval. Top panels: Rolled fingerprints. Middle panels: Latent fingerprints. Bottom panels: Retrieved fingerprints.

Table 1. Latent pattern retrieval for a T-Grid network with $N = 89{,}420$, $K = 224$, $\omega = 0.4$, $\alpha = 0.05$.

Fingerprint	m^0 (latent fingerprint overlap)	m^* (matched fingerprint overlap)	Time
FP1	0.097977	0.949862	52
FP2	0.186651	0.921409	30
FP3	0.264667	0.980916	17
FP4	0.145478	0.948081	99
FP5	0.294989	0.995920	11

fingerprints (middle panels of Fig. 7), come from a different acquisition of the same fingers of the rolled set of fingerprints stored by the network. The network manages to match the latent fingerprints to the corresponding rolled ones, as presented in the bottom panels of Fig. 7.

In Table 1 is presented the initial overlap m^0 for the latent fingerprints used as initial condition. The final overlaps m^* after the network evolution are also presented, as well as, the time steps to reach a steady state. Starting with an initial overlap as low as 9.8% in the FP1 example, after $t = 52$ time retrieval steps, the network manages to match the final state to the corresponding latent fingerprint with a final overlap of $m^* \sim 95\%$. One can appreciate that the network retrieval abilities are robust when starting with latent fingerprints which are incomplete, stretched or slightly rotated, as the ones presented in the middle row of Fig. 7.

The metric ANN presented in this work has proved valuable for denoising and completion of fingerprint patterns as the ones depicted in Fig. 1. Also, for true noise latent fingerprints as the ones presented in middle panels of Fig. 7. The proposed

model may be helpful for latent fingerprint identification, which is very relevant for forensic applications as shown by Paulino *et al.*[36]

5. Conclusion and Discussion

In this paper, we have proposed a diluted metric attractor neural network to store and retrieve collections of fingerprint images. We tested this network in different topological configurations. This network uses a connectivity distribution which is modulated by two parameters: the connectivity ratio and the randomness ratio. Unlike some approaches of Hopfield neural networks, using metric networks we can increase the ROI to cover almost the complete fingerprint. One must be aware that the network was chosen to be very diluted, allowing for the storage of larger size patterns than a fully connected network does, given the same memory amount is at disposal. Our approach has been successfully tested for different types of noisy configurations of the fingerprints, and the network proved to be robust with a large basin of attraction. We studied the retrieval capacities for noiseless fingerprints, as well as different noisy configurations of the fingerprint patterns. Our results have shown that the 2D topology configurations (C-Grid, X-Grid, T-Grid) performed better retrieval capacities than the 1D-Ring configuration (see Fig. 3). We calculated the network phase diagram for the parameters randomness ratio versus load ratio, for the different topological configurations. All 2D configurations outperforms the Ring configuration, for values of $\omega < 0.2$ the X-Grid configuration performs better and for larger values of ω the T-Grid is the winner. A phase diagram was also calculated for the different noisy initial conditions considered in this work. The more representative result is that for noiseless ($m^0 = 1.0$) and for the different noisy initial conditions, i.e. uniform noise ($m^0 = 0.2$), the optimal randomness ratio is between $\omega = 0.6$ and $\omega = 0.7$. We think that these network configurations better represent the intrinsic spatial structure of the fingerprints as shown in the phase diagrams.

Also, we pointed out a "detective" application related with pattern overlap crossing for fingerprint matching. We showed that the dynamical properties of the metric network can help to distinguish between two fingerprint candidates which could be attributed to the same individual. In fact, by presenting an initial candidate pattern which is apparently less similar (with lower overlap) to the reference fingerprint stored by the network, the dynamical evolution leads to a final network state that matches better to the corresponding reference fingerprint. This is shown by the Supplanter and Intended initial patterns overlap crossing evolution in Fig. 6. This feature could be very useful for fingerprint verification in order to discriminate between fingerprint pairs.

Finally, we presented examples of latent fingerprint matching, coming from a different acquisition of the same rolled finger impression stored by the network. The network proved to be very robust matching the right fingerprint from incomplete, stretched and slightly rotated latent fingerprints with initial overlap as low as 9.8%. A more detailed study of our approach applied to recognition of latent fingerprints (i.e. captured from a crime scene) warrants further investigation.

Acknowledgments

This work has been funded by the Spanish Government (MICINN) under Projects TIN2011-29827-C02-01 and TIN-2010-19607. M. González thanks UNEMI 2014 CONVP01-012 and EM-ECW Lot 20 for financial support.

References

1. D. Maltoni, D. Maio, A. K. Jain and S. Prabhakar, *Handbook of Fingerprint Recognition*, 2nd edn. (Springer Publishing Company, Incorporated, 2009).
2. A. K. Jain, A. A. Ross and K. Nandakumar, *Introduction to Biometrics* (Springer, 2011).
3. A. K. Jain, S. Prabhakar and S. Pankanti, On the similarity of identical twin fingerprints, *Pattern Recogn.* **35**(11) (2002) 2653–2663.
4. R. Bolle, J. Connell, S. Pankanti, N. Ratha and A. Senior, *Guide to Biometrics* (Springer-Verlag, 2005).
5. F. Alonso-Fernandez, J. Fierrez, J. Ortega-Garcia, J. Gonzalez-Rodriguez, H. Fronthaler, K. Kollreider and J. Bigun, A comparative study of fingerprint image-quality estimation methods, *IEEE Trans. Inf. Forensics Security* **2**(4) (2007) 734–743.
6. D. Benini *et al.*, ISO/IEC 29794-1 Biometric sample quality standard: Framework (2008).
7. A. Meraoumia, S. Chitroub and A. Bouridane, 2d and 3d palmprint information, PCA and HMM for an improved person recognition performance, *Integr. Comput. Aided Eng.* **20**(3) (2013) 303–319.

8. A. K. Jain and J. Feng, Latent fingerprint matching, *IEEE Trans. Pattern Anal. Mach. Intell.* **33**(1) (2011) 88–100.
9. A. A. Mohammed, R. Minhas, Q. M. Johnathan Wu and M. A. Sid-Ahmed, An efficient fingerprint image compression technique based on wave atoms decomposition and multistage vector quantization, *Integr. Comput. Aided Eng.* **17**(1) (2010) 29–40.
10. Y. Amit and M. Mascaro, Attractor networks for shape recognition, *Neural Comput.* **13** (1999) 1415–1442.
11. W. Fink, Neural attractor network for application in visual field data classification, *Phys. Med. Biol.* **49**(13) (2004) 2799.
12. M. González, D. Dominguez and Á. Sánchez, Learning sequences of sparse correlated patterns using small-world attractor neural networks: An application to traffic videos, *Neurocomputing* **74**(14–15) (2011) 2361–2367.
13. W.-Y. Hsu, Application of competitive Hopfield neural network to brain-computer interface systems, *Int. J. Neural Syst.* **22**(1) (2012) 51–62.
14. F. Han, M. Wiercigroch, J.-A. Fang and Z. Wang, Excitement and synchronization of small-world neuronal networks with short-term synaptic plasticity, *Int. J. Neural Syst.* **21**(5) (2011) 415–425.
15. D. Dominguez, M. González, E. Serrano and F. B. Rodríguez, Structured information in small-world neural networks, *Phys. Rev. E* **79**(2) (2009) 021909.
16. M. González, D. Dominguez and F. B. Rodríguez, Block attractor in spatially organized neural networks, *Neurocomputing* **72**(16–18) (2009) 3795–3801.
17. D. Dominguez, M. González, F. B. Rodriguez, E. Serrano, R. Erichsen Jr. and W. K. Theumann, Structured information in sparse-code metric neural networks, *Physica A* **391**(3) (2012) 799–808.
18. K. Koroutchev and E. Koroutcheva, Bump formation in a binary attractor neural network, *Phys. Rev. E* **73** (2006) 026107.
19. Y. Roudi and A. Treves, An associative network with spatially organized connectivity, *J. Stat. Mech.* **2004**(7) (2004) P07010.
20. Y. Roudi and A. Treves, Localized activity profiles and storage capacity of rate-based autoassociative networks, *Phys. Rev. E* **73** (2006) 061904.
21. Y. Roudi and A. Treves, Representing where along with what information in a model of a cortical patch, *PLoS Comput. Biol.* **4**(3) (2008) e1000012.
22. D. Dominguez, K. Koroutchev, E. Serrano and F. B. Rodríguez, Information and topology in attractor neural networks, *Neural Comput.* **19** (2007) 956–973.
23. M. M. Rashid and A. K. Hossain, Fingerprint verification system using artificial neural network, *Inf. Tech. J.* **5**(6) (2006) 1063–1067.
24. K. Ahmadian and M. Gavrilova, Using duality and Hopfield neural network for Delaunay triangulation based fingerprint matching, *ICC'09. Int. Conf. Computing, Engineering and Information* (2009), pp. 225–230.
25. A. N. Ouzounoglou, T. L. Economopoulos, P. A. Asvestas and G. K. Matsopoulos, Using duality and Hopfield neural network for Delaunay triangulation based fingerprint matching, *XII Mediterranean Conf. Medical and Biological Engineering and Computing* (2010), pp. 307–310.
26. P. Baldi and Y. Chauvin, Neural networks for fingerprint recognition, *Neural Comput.* **5**(3) (1993) 402–418.
27. S. Bernard, N. Boujemaa, D. Vitale and C. Bricot, Fingerprint classification using Kohonen topologic map, in *IEEE Int. Conf. on Image Processing, ICIP* (Thessaloniki, Greece, 2001), pp. 230–233.
28. K. N. Mutter, Z. M. Jafri and A. A. Aziz, Automatic fingerprint identification using gray Hopfield neural network improved by run-length encoding, in *Fifth Int. Conf. Computer Graphics, Imaging and Visualisation, 2008. CGIV'08.* August 2008, pp. 205–210.
29. C. Hillar, J. Sohl-Dickstein and K. Koepsell, Efficient and optimal binary Hopfield associative memory storage using minimum probability flow, arXiv:1204.2916 (2012).
30. M. M. Cappelli, D. Maio, D. Maltoni, J. L. Wayman and A. K. Jain, FVC2004: Third fingerprint verification competition, in *Proc. First Int. Conf. Biometric Authentication* (2004), p. 17.
31. S. Chikkerur, A. N. Cartwright and V. Govindaraju, Fingerprint enhancement using STFT analysis, *Pattern Recogn.* **40**(1) (2007) 198–211.
32. D. J. Watts and S. H. Strogatz, Collective dynamics of "small-world" networks, *Nature* **393** (1998) 440–422.
33. T. J. Strain, L. J. McDaid, T. M. McGinnity, L. P. Maguire and H. M. Sayers, An STDP training algorithm for a spiking neural network with dynamic threshold neurons, *Int. J. Neural Syst.* **20**(6) (2010) 463–480.
34. A. Montero, R. Huerta and F. B. Rodríguez, Neuron threshold variability in an olfactory model improves odorant discrimination, *IWINAC* (1) (2013), pp. 16–25.
35. D. Dominguez and D. Bollé, Self-control in sparsely coded networks, *Phys. Rev. Lett.* **80** (1998) 2961–2964.
36. A. A. Paulino, J. Feng and A. K. Jain, Latent fingerprint matching using descriptor-based Hough transform, *IEEE Trans. Inf. Forensics Security* **8**(1) (2013) 31–45.
37. J. Feng, Y. Shi and J. Zhou, Robust and efficient algorithms for separating latent overlapped fingerprints, *IEEE Trans. Inf. Forensics Security* **7**(5) (2012) 1498–1510.
38. Q. Zhao and A. K. Jain, Model based separation of overlapping latent fingerprints, *IEEE Trans. Inf. Forensics Security* **7**(3) (2012) 904–918.